

Nanofabrication of Plasmonic Structures*

Joel Henzie, Jeunghoon Lee, Min Hyung Lee,
Warefta Hasan, and Teri W. Odom

Department of Chemistry and Materials Science and Engineering, Northwestern University,
Evanston, Illinois 60208; email: todom@northwestern.edu

Annu. Rev. Phys. Chem. 2009. 60:147–65

First published online as a Review in Advance on
October 17, 2008

The *Annual Review of Physical Chemistry* is online at
physchem.annualreviews.org

This article's doi:
10.1146/annurev.physchem.040808.090352

Copyright © 2009 by Annual Reviews.
All rights reserved

0066-426X/09/0505-0147\$20.00

*The U.S. Government has the right to retain a
nonexclusive, royalty-free license in and to any
copyright covering this paper.

Key Words

multiscale patterning, nanohole arrays, pyramidal nanoparticles, surface plasmons, refractive-index sensing

Abstract

This review focuses on nanofabrication tools, based on soft lithography, which can generate a wide range of noble-metal structures with exceptional optical properties. These techniques offer a scalable and practical approach for producing arrays of complementary plasmonic structures (nanoholes and nanoparticles) and, in addition, expand the possible architectures of plasmonic materials because the metal building blocks can be organized over multiple length scales. We describe the preparation and characterization of five different systems: subwavelength nanohole arrays, finite arrays of nanoholes, microscale arrays of nanoholes, multiscale arrays of nanoparticles, and pyramidal particles. We also discuss how the surface plasmon resonances of these structures can be tuned across visible and near-infrared wavelengths by varying different parameters. Applications and future prospects of these nanostructured metals are addressed.

Enhanced optical transmission:

phenomenon in which the amount of light transmitted through subwavelength hole arrays is greater than that permitted by geometric optics

Subwavelength hole arrays:

metal films perforated with holes whose sizes and spacings are much less than the wavelength of incident light

Surface plasmon polaritons (SPPs):

longitudinal surface charge density waves of conduction electrons coupled to light

INTRODUCTION

Plasmonics encompasses the science and applications of noble-metal structures that can guide and manipulate visible light at the nanometer scale. The recent, rapid pace of discoveries in plasmonics can be attributed to three cooperative factors: making, measuring, and modeling (1). First, advances in both synthetic and fabricated approaches to creating nanostructures have allowed control over the shape and size of metal structures (**Figure 1**). In particular, the development of nanofabrication tools capable of sub-100-nm resolution has played a key role in enabling groundbreaking observations, including the demonstration of enhanced optical transmission through subwavelength hole arrays (2), the collimation of light through a subwavelength bull's-eye structure (3), negative permeability and refraction at visible wavelengths (4, 5), and second harmonic generation from magnetic metamaterials (6). Second, imaging tools, including near-field scanning optical microscopy, have enabled the direct imaging of surface plasmon polariton waves (7), and optical microscopes equipped with single-particle spectroscopy capabilities have allowed localized surface plasmon resonances to be correlated with individual metal particles (8). Lastly, advances in theoretical tools, including optimized electrodynamic calculation methods and improved computational resources, have made descriptions (and often predictions) of the optical properties possible (9, 10).

Brief Primer on Surface Plasmons

The optical properties of metals are determined in part by the resonant interaction between light and their surface free electrons at a metal-dielectric interface. These collective electron oscillations—surface plasmon polaritons (SPPs)—exist as propagating waves on planar metal films (**Figure 2a**) with amplitudes that extend further into the dielectric region compared with the metal region. To excite SPPs on a surface using free-space light, one must provide additional momentum either by the patterning of a grating structure on the film or by the evanescent coupling of light into the metal (11). The propagation distance of SPPs depends primarily on the absorption of the metal and the thickness and surface roughness of the film; for SPPs on Au films excited using 633-nm light, this decay length is approximately 10 μm (12, 13).

Metal particles (<250 nm in diameter) also interact strongly with light through plasmon resonances that are confined within 10 nm of the particle surface (**Figure 2b**), usually at a point or

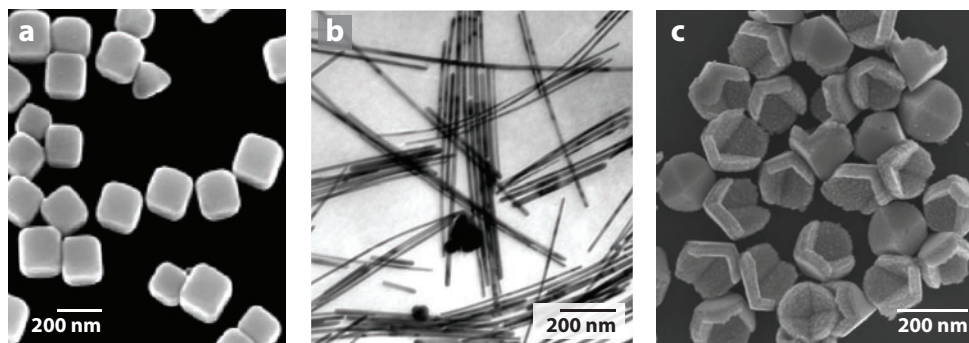


Figure 1

Plasmonic nanostructures: (a) scanning electron microscopy (SEM) image of Ag cubes, (b) transmission electron micrograph of Ag nanowires, and (c) SEM image of Au/Ni pyramids. Panel a reprinted with permission from Reference 56, copyright (2004), Wiley. Panel b reprinted with permission from Reference 57, copyright (2001), Royal Society of Chemistry.

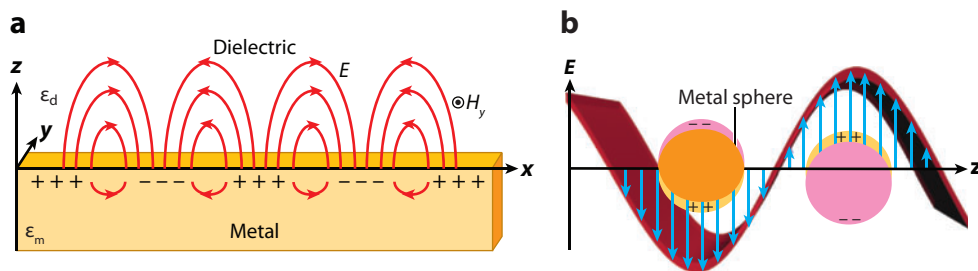


Figure 2

Different types of surface plasmons: (a) surface plasmon polaritons at a metal-dielectric interface and (b) localized surface plasmons on a metal nanoparticle excited by free-space light.

a tip; these resonant optical fields are called localized surface plasmons (LSPs). LSP resonances are highly sensitive to the size (14), shape (15), and dielectric environment of the metal particles and can be tuned from ultraviolet (UV) to near-infrared (NIR) wavelengths (16). Spherical particles with sizes less than 50 nm support single LSP resonances that are dipolar in character, and their optical properties can be described reasonably well by the lowest order term in Mie theory (17). Larger metallic particles (overall sizes greater than 100 nm) with anisotropic shapes can exhibit multiple LSP resonances (18, 19) that correspond to higher-order plasmon modes (20). For example, 100-nm-diameter Au pyramids exhibit only a dipole resonance in contrast to identically shaped pyramids with sizes of 250 nm or larger that support higher-order, multipolar modes (21). These multipolar excitations depend on the direction of the wave vector, as well as the polarization vector (22); thus, certain excitation angles can allow selected resonances to be more pronounced (23). Rod-shaped Au nanoparticles can also support both transverse and longitudinal modes, depending on polarization (24, 25).

Conventional Methods for Generating Plasmonic Structures

Chemical synthesis has been the primary means of growing a wide variety of metal nanoparticle shapes (including stars, rods, boxes, and cages) because reaction conditions such as temperature, surfactants, and precursors can be independently controlled (26). Extensive overviews of the different synthetic conditions and outcomes have been published elsewhere (15, 25). Although solution-based methods are scalable, the large distribution in nanoparticle shape and size within a single reaction vessel is still a challenge. Metal particles can also be assembled into two-dimensional (2D) and 3D lattices using a variety of techniques; both the interparticle distances and the geometry of the lattices can be used to tune the optical properties of the assemblies (27–30).

Nanofabrication methods offer an alternative strategy of organizing plasmonic structures into arrays. Direct-write techniques such as electron-beam lithography can fabricate linear and 2D arrays of nanoparticles with different spacings (31, 32), which typically need to be on the order of the size of the particle or less (<200 nm) for efficient dipolar coupling (33). Focused ion beam milling has been the most common method for fabricating hole and slot structures in optically thick metal films (2). This method can drill completely or partially through the film and can control the diameter and spacing of the structures with reasonable precision (approximately 100 nm). Free-standing suspended films have also been fabricated by focused ion beam milling and reactive ion etching, but the generation of multilayered metal films is difficult and laborious (34). Besides these direct-write methods, templates have been the primary method of producing particles with anisotropic shapes. Isolated submicrometer spheres and close-packed sphere arrays can act as

Localized surface plasmons (LSPs): collective oscillations of surface conduction electrons confined to a finite volume

Soft lithography:

fabrication techniques that use an elastomeric stamp as the pattern-transfer element

Multiscale patterning:

simultaneous patterning of nanoscale, microscale, and macroscale features

Soft interference lithography (SIL):

nanofabrication technique that uses nanopatterns made by interference lithography as masters for soft lithography

IL: interference lithography

templates onto which metals can be deposited to obtain particles with crescent-like shapes (35, 36) and truncated triangular prisms (37). Anodized aluminum-oxide membranes compose another widely used template for producing nanorods as long as 10 μm (38). Investigators have also used etched Si templates and nanohole masks to create pyramidal shells (27, 30).

This article focuses on how new types of nanofabrication tools, based on soft lithography, can generate a wide range of plasmonic structures with exceptional optical properties. There are two important features of these techniques: (a) They provide a scalable and inexpensive approach for creating arrays of complementary metal structures (nanoholes and nanoparticles), and (b) they expand the types of plasmonic metamaterials that are possible because the metal building blocks can now be organized over multiple length scales and over macroscale areas. The most pressing reason that multiscale patterning is critical for designing and understanding new plasmonic systems is that surface plasmons interact over multiple length scales: tens of nanometers for LSPs and tens of micrometers for SPPs. The interplay between LSPs and SPPs—and SPPs with other SPPs—has not been studied extensively, however, because conventional methods cannot easily produce the necessary metal patterns and architectures.

A PLATFORM FOR MULTISCALE NANOSCALE PATTERNING

We have invented a variation of soft lithography—soft interference lithography (SIL)—that can be used to generate plasmonic nanostructures over wafer-scale areas. Soft lithography is a catch-all term for fabrication techniques that use macroscopic poly(dimethylsiloxane) (PDMS) stamps or masks to transfer patterns from one material or surface to another (29). To produce sub-100-nm features, investigators improved the mechanical properties of PDMS (28) and developed composite PDMS masks comprising a thin, stiff layer of hard *b*-PDMS supported by a slab of 184 PDMS (39, 40). Soft lithographic methods offer three important advantages over serial ones: parallelism, simplicity, and flexibility. PDMS molded against a master forms a transparent, elastomeric mask that can be used to create arrays of structures simultaneously. Moreover, only widely available microfabrication tools are required, such as photolithography, wet chemical etching, electron-beam deposition, reactive ion etching, and microtomy (41). Finally, one can generate patterns with various symmetries and array spacings; out of multiple, different materials; and with exquisite control over the thickness of each layer.

Soft Interference Lithography: Patterns on a Nanoscale Pitch

SIL uses nanoscale patterns generated by interference lithography (IL) as high-quality masters for soft lithography (42). **Figure 3a** shows an IL master patterned with Si posts. Hundreds of SIL photomasks can be replicated from one master pattern without exhibiting observable defects. To produce patterns in a photoresist identical in size and shape to the IL master, one places the SIL photomask in conformal contact with a positive-tone photoresist and then exposes it with broadband UV light. If the photoresist is developed at this point, posts with the same lateral dimensions as the IL master (referred to as infinite arrays) are produced. If the photoresist is exposed again through a Cr photomask patterned with microscale (1–10- μm) features and then developed, patches of post arrays (referred to as finite arrays) form. The overall size of an SIL master is typically large (>2 inches²) and thus can be aligned with the top edge of a Cr photomask to achieve misalignments less than 5% in rotation; the use of a mask aligner reduces misalignments to less than 1%.

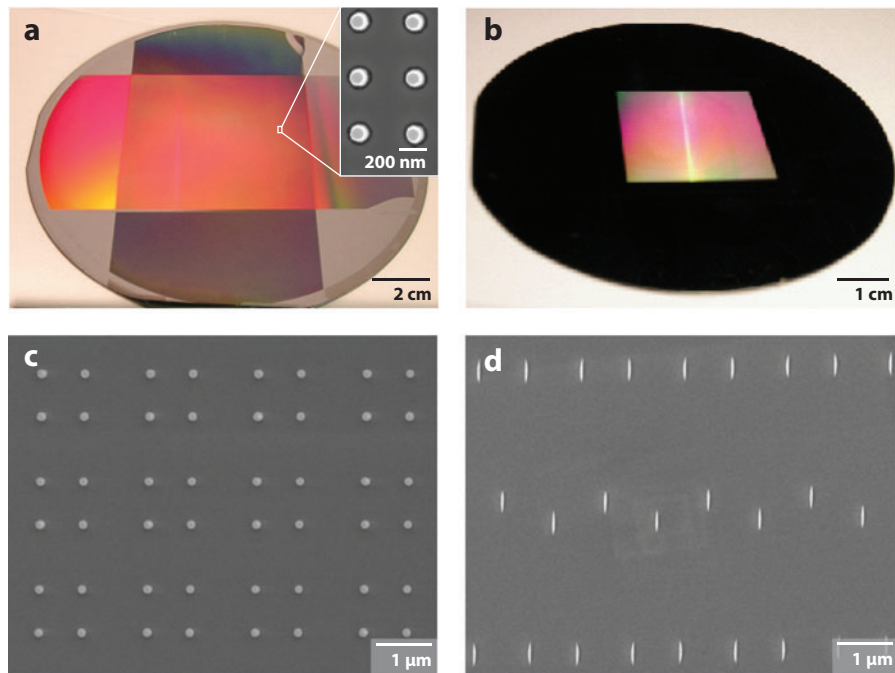


Figure 3

Masters with macroscale dimensions patterned with nanoscale features. (a) Si master made by interference lithography. The Si posts are 400 nm tall, 100 nm in diameter, and on a square array of $a_0 = 400$ nm. (b) Photoresist master made by phase-shifting photolithography. The photoresist posts are on a microscale pitch and can be (c) circular, 400 nm tall, and 250 nm in diameter or (d) anisotropic, 400 nm tall, and $90 \text{ nm} \times 900 \text{ nm}$ in size. Panel a reprinted with permission from Reference 42, copyright (2007) Nature Publishing.

Phase-Shifting Photolithography: Patterns on a Microscale Pitch

Standard phase-shifting photolithography (PSP) is an edge photolithography technique that produces narrow features in a photoresist at the edges of the patterns in a PDMS mask. Typically, these PSP masks are fabricated by replicating photoresist masters ($b = 400$ nm) with microscale ($a_0 = 1\text{--}25 \text{ } \mu\text{m}$, $d = 1\text{--}25 \text{ } \mu\text{m}$) patterns (Figure 3b). One can produce edge features as narrow as 50 nm in a positive-tone photoresist by exposing UV light through a composite PDMS mask. When two exposures are made through a mask patterned with microscale lines (the mask is rotated after the first exposure and then exposed again before development), photoresist posts form at the intersection of the line patterns (40, 43). If the second exposure occurs through the same mask and is rotated by 90° , square arrays of circular dots form; when rotated by 15° , more complex arrays of anisotropic posts form (the smallest distance between dots is determined by the periodicity of the line mask) (Figure 3c,d) (44).

PEEL: Transferring Photoresist Patterns to Plasmonic Materials

PEEL (a method combining PSP, etching, electron-beam deposition, and lift-off) is a nanopatterning procedure that transfers patterned features in a photoresist into free-standing, functional materials (Figure 4) (12, 45). First, one uses PSP to define the photoresist pattern on an Si(100) surface, and then deposition and lift-off transfer the photoresist pattern onto holes in a Cr film.

PSP: phase-shifting photolithography

PEEL: phase-shifting photolithography, etching, electron-beam deposition, lift-off; a nanofabrication procedure that produces free-standing nanostructures from a patterned photoresist

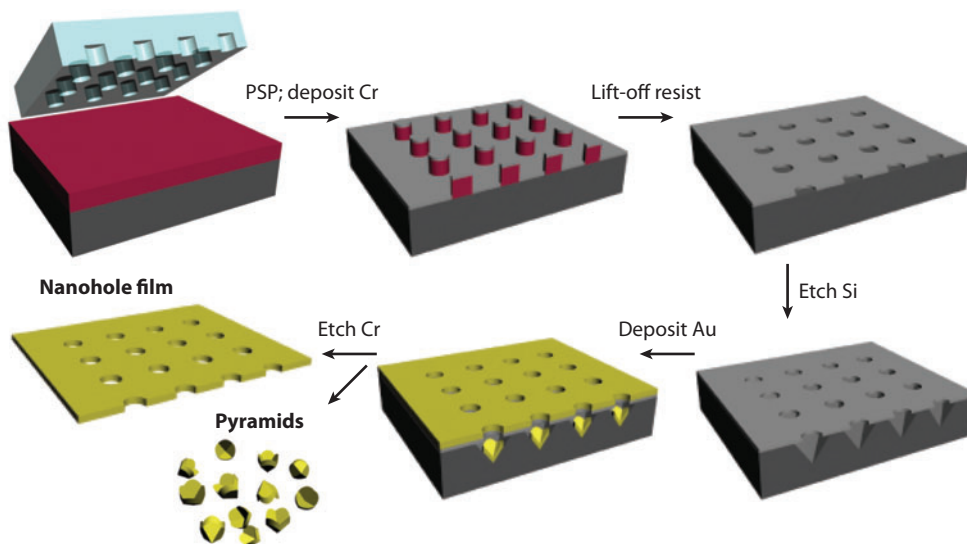


Figure 4

PEEL [phase-shifting photolithography (PSP), etching, electron-beam deposition, and lift-off] procedure to transfer patterns in a photoresist to functional materials such as Au or Si. Arrays of nanoscale holes and arrays of pyramidal nanoparticles are fabricated simultaneously.

The film of Cr holes acts as an etch mask to form pyramidal pits in the Si(100) surface beneath the holes and then as an electron-beam deposition mask to produce perforated metal films over pyramidal particles. The metal nanohole film can be released from the surface by etching the Cr layer and placing the film on a glass substrate. The nanopyrramids formed within the Si pits can be embedded in other materials such as PDMS (21) or released from the Si template, suspended in solution, and dispersed on a substrate (27).

SUBWAVELENGTH ARRAYS OF NANOHOLE

In the early twentieth century, the intensity of transmission through subwavelength apertures in opaque metal films was expected to be small, proportional to $(r/\lambda)^4$ based on geometric optics (46). The discovery of enhanced optical transmission through subwavelength hole arrays exceeded these predictions by orders of magnitude (2) and, moreover, revealed that the wavelengths of highest transmission could be tuned by changing the material of the film, the hole size, and the array spacing and geometry (47). Surface plasmons play a critical role in enhanced transmission. Light incident on the hole array excites surface plasmons on one side of the film, which then tunnel through the holes and/or increase the efficiency of light transmitted through the holes. Then, the surface plasmons that emerge at the opposite side of the film scatter from the hole array structure and are converted into free-space light (48).

Infinite Arrays of Nanoholes

We define subwavelength nanohole arrays as metal films perforated by holes whose diameter and spacing are smaller than the wavelength of incident and transmitted light. We fabricated macroscale areas of films perforated with arrays of 100-nm-diameter circular holes using SIL and PEEL and placed them on a glass substrate (refractive index $n = 1.523$) (Figure 5a). The optical properties were characterized by illuminating the nanohole arrays under normal incidence with collimated

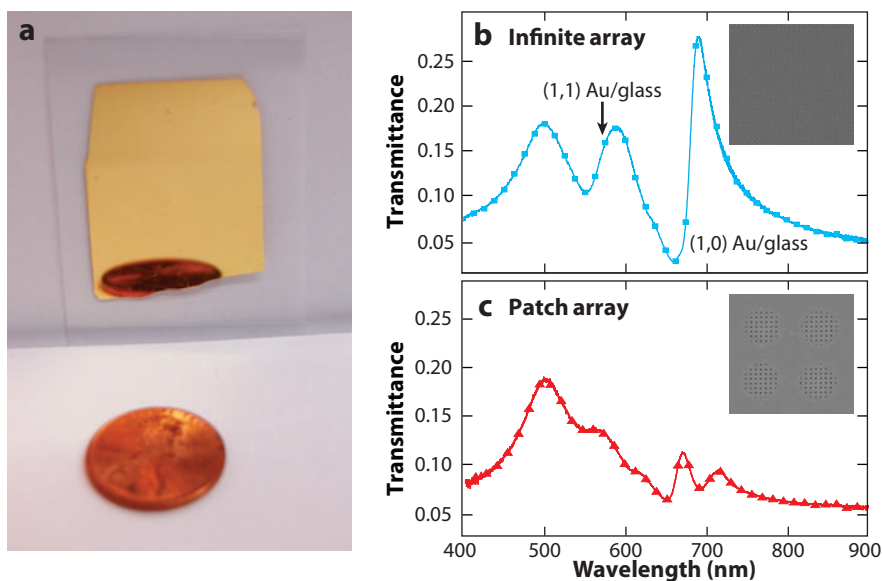


Figure 5

Macroscale areas of Au films perforated with 100-nm holes. (a) Optical micrograph of an Au nanohole array supported on glass. (b) Zero-order transmission spectra of an infinite Au nanohole array. The Au film is 50 nm thick. The surface plasmon Bloch modes are labeled (1,0) and (1,1) and correspond to the (i, j) pairs at the relevant metal-dielectric interface. (c) Zero-order transmission spectra of a patch Au nanohole array. The patches are separated by 4.5 μm . Figure adapted and reproduced with permission from Reference 42, copyright (2007) Nature Publishing.

white light and then collecting the transmitted light through a microscope objective coupled to a spectrometer. When the incident light is normal to a square array of nanoholes of periodicity a_0 in an Au film, an approximate equation for the SPP Bloch wave modes (λ_{SPP}) is given by

$$\lambda_{\text{SPP}} = \frac{a_0}{\sqrt{i^2 + j^2}} \sqrt{\frac{\varepsilon_{\text{Au}} \varepsilon_d}{\varepsilon_{\text{Au}} + \varepsilon_d}},$$

where i and j are integers that define the particular order of the Bloch modes, ε_{Au} is the permittivity of Au, and ε_d is the permittivity of the adjacent dielectric material (superstrate or glass substrate) (49).

Figure 5b indicates that infinite Au nanohole arrays exhibit peaks characteristic of SPPs at the Au/glass interface of $\lambda_{\text{SPP}}(1,0) = 690$ nm and $\lambda_{\text{SPP}}(1,1) = 588$ nm, where (1,0) and (1,1) correspond to the (i, j) pairs. The minimum in the spectra $\lambda = 659$ nm can be associated with a Wood's anomaly (light diffracted parallel to the surface) (50), and the peak at 500 nm is the bulk plasmon resonance of an Au film. Compared with the calculated transmission of hole arrays based only on geometry, the infinite Au nanohole arrays exhibit enhanced optical transmission factors as large as 11, indicating that SIL can produce hole arrays of optical quality at least equal to those fabricated by focused ion beam milling. **Figure 6** shows how one can tune the properties of the Au infinite subwavelength nanohole arrays by changing the refractive index of the top surface from air ($n = 1$) (**Figure 5b**) to different refractive-index oils ($n = 1.5$ to 1.7). As expected, the SPP peaks of the infinite Au nanohole arrays red-shifted with increased n , but the bulk plasmon remained unchanged. Numerical calculations revealed that at $n = 1.7$, the peak at $\lambda = 563$ nm is a localized resonance; the peak at $\lambda = 620$ nm is the (1,1) Au/oil resonance; the sharp peak at

SPP Bloch wave modes: propagating SPP modes on a periodically structured surface

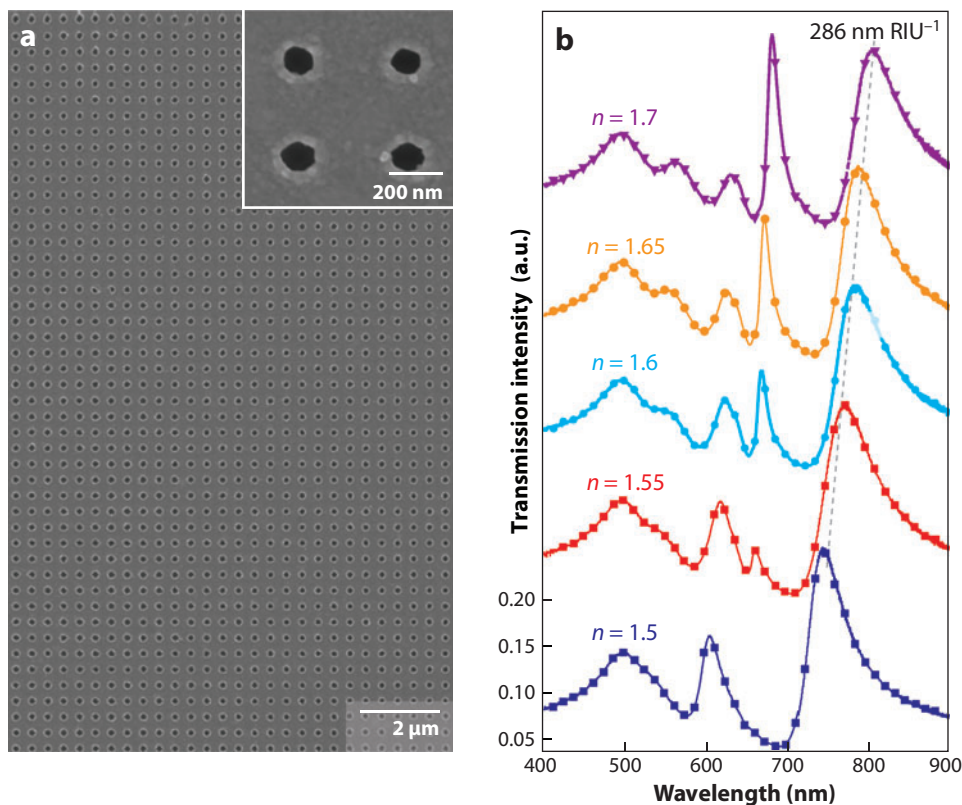


Figure 6

Refractive index sensing using infinite Au nanohole arrays. (a) Scanning electron micrograph of a portion of the infinite Au nanohole array. (b) Zero-order transmission of infinite Au hole arrays on glass in the presence of higher-index immersion oils ($n = 1.50$ – 1.70). Figure reproduced with permission from Reference 42, copyright (2007) Nature Publishing.

$\lambda = 681$ nm arises, in part, from first-order diffraction; and the peak at approximately 800 nm can mostly be attributed to the (1,0) Au/oil resonance (51).

Finite Arrays (Patches) of Nanoholes

Light transmitted through subwavelength apertures should diffract in all directions (46). The relationship between the enhanced optical transmission of light and its spatial output, however, suggests that light traveling through subwavelength holes can be manipulated. Hence, we designed microscale patches (overall sizes ranging from $d = 2.5$ to $10 \mu\text{m}$) of 100-nm holes to test how light emerged from these structures. Interestingly, light transmitted most strongly from the center of the patches and appeared to focus to a point; the wavelength-dependent intensity of these spots also correlated with the plasmon resonances of the finite arrays of nanoholes (42). This result has important implications because it suggests that plasmons—an inherently near-field phenomena—can strongly affect the overall geometry of the far-field transmission pattern (3).

Figure 7a shows that finite-sized nanohole arrays patterned into circular regions ($d = 2.5 \mu\text{m}$, $a_0 = 4.5 \mu\text{m}$) of patches contained ~ 30 nanoholes. Because the size and pitch of the circles on the Cr mask were incommensurate with the photoresist post lattice (400 nm), neighboring patches had

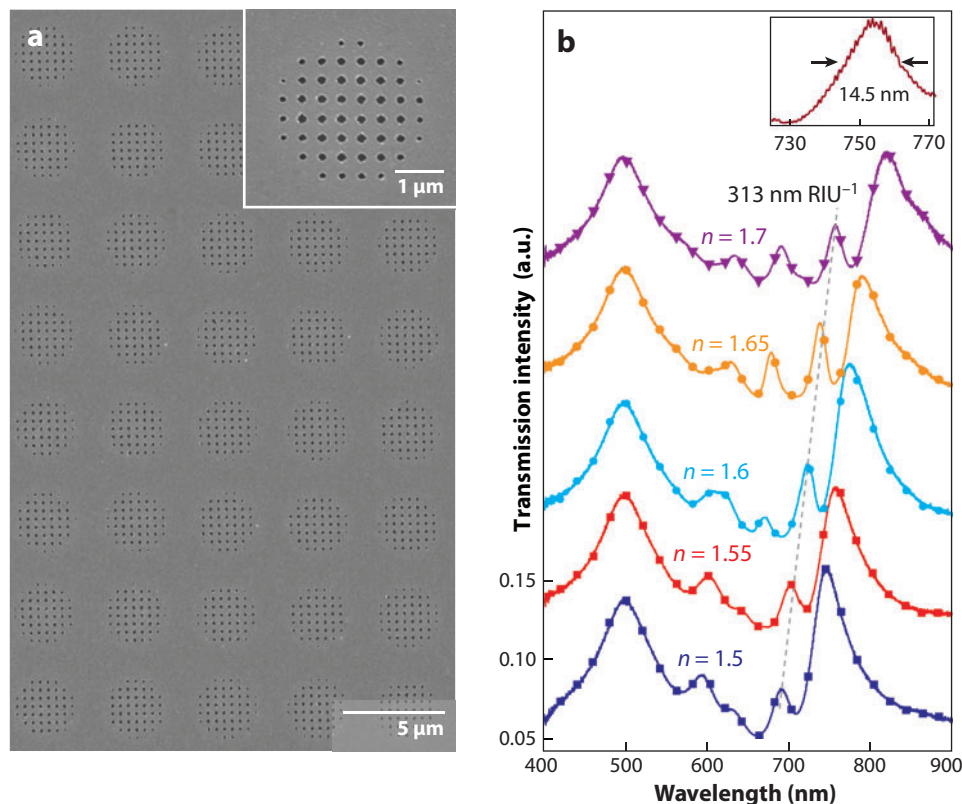


Figure 7

Refractive index sensing using patches of Au nanohole arrays. (a) Scanning electron micrograph of a portion of an array of 2.5- μm Au patches of nanoholes separated by 4.5 μm . (b) Zero-order transmission of Au patches on glass in the presence of higher-index immersion oils ($n = 1.50\text{--}1.70$). Figure reproduced with permission from Reference 42, copyright (2007) Nature Publishing.

slightly different hole configurations. The spectra acquired for single patches indicated, however, that these small structural variations did not noticeably affect the optical properties. Compared with the infinite hole array in **Figure 5b**, **Figure 5c** shows that the nanohole patch spectra with an air superstrate exhibited a new, narrow peak at $\lambda = 660$ nm (full width at half-maximum of 16.8 nm) as well as a decrease in the relative intensity of the (1,0) resonance. Also, similar to the infinite arrays, all the SPP peaks shifted to longer wavelengths when the refractive index of the superstrate increased from air to different index oils. Noticeably, several peaks remained very narrow over the range of n tested (**Figure 7b**); for example, the peak that shifted from $\lambda = 690$ nm ($n = 1.5$) to $\lambda = 756$ nm ($n = 1.7$) had an average full width at half-maximum of 14.8 ± 0.6 nm, which is one of the narrowest spectral widths reported for a surface plasmon resonance.

MICROSCALE ARRAYS OF NANOSCALE HOLES

Although most work to date has focused on subwavelength hole arrays (in which both the size of the holes and the spacing of the array are subwavelength in scale), nanoscale holes patterned with microscale spacings (microscale arrays) are becoming important for understanding in detail the optical properties of nanostructured metallic surfaces (12, 45). Such structures—whose

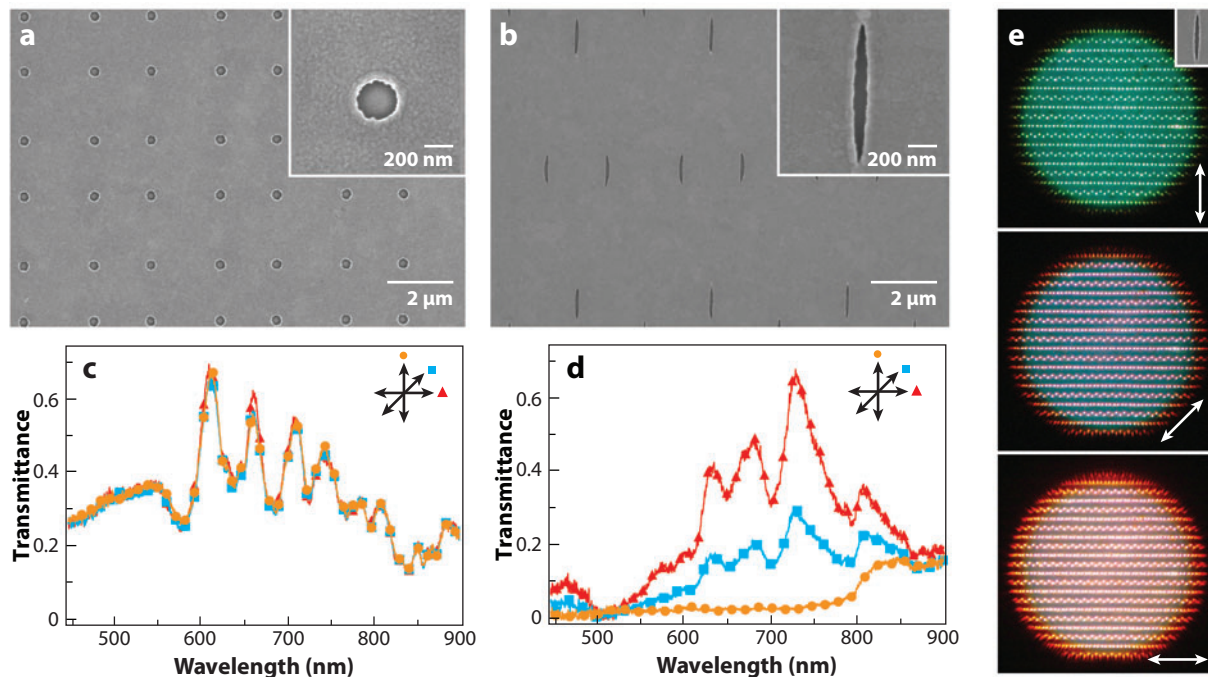


Figure 8

Microscale arrays of nanoscale holes. Nanohole arrays in 170-nm-thick Au films perforated with (a) circular and (b) slit-like holes. Zero-order transmittance of arrays of (c) 250-nm circular holes and (d) slit-like holes under illumination of light with different polarizations: $\theta = 0^\circ$ (orange circles), 45° (blue squares), and 90° (red triangles). (e) Bright-field optical micrographs of colors transmitted by the slit-like holes shown in panel b under different polarizations of incident light. Figure adapted and reprinted with permission from Reference 54, copyright (2007) Wiley.

hole-hole spacing is greater than the wavelength of incident light—show unique spectral characteristics compared with subwavelength hole arrays because of high-order Bragg coupling. Furthermore, anisotropic nanoholes patterned into different geometries display striking, tunable polarization-dependent colors (44).

Figures 8a,b depict 170-nm-thick Au films perforated with 250-nm circular holes in a square array ($\phi = 90^\circ$) and 90 nm \times 950-nm slit-like holes in a sharp-diamond array ($\phi = 15^\circ$) made by PSP followed by PEEL. **Figure 8c** indicates that circular holes in microscale arrays exhibit markedly different optical transmission characteristics in the visible wavelength range compared with subwavelength nanohole arrays (**Figure 5b**). The microscale spacing of the array produced ultranarrow features in the transmittance (some had a full width at half-maximum of less than 15 nm) because of high-order Bragg modes, in which the square lattice has a spacing of $a_0 = 4 \mu\text{m}$ (the unit cell size, because the two sets of spacings are 1.8 μm and 2.2 μm). Thus, the SPP-Bragg modes are constrained by $17 \leq (i^2 + j^2) \leq 58$ at the Au/air interface and $40 \leq (i^2 + j^2) \leq 200$ at the Au/glass interface in the range of 550–950 nm. High-order surface plasmon Bragg modes are thus expected with microscale arrays, in contrast with the low-order modes [e.g., (1,0) and (1,1)] observed in subwavelength nanohole arrays. Similar to circular hole arrays, anisotropic hole arrays (with a larger and more complicated unit cell) exhibit complex spectral features (**Figure 8d**).

Circular nanohole arrays illuminated with polarized white light transmitted color that appeared yellowish-white, and no noticeable difference was observed under polarization because of the

symmetry of the holes. In contrast to circular holes, slit-like hole arrays exhibited dramatic color changes tunable from green to red as the polarization direction of the incident light rotated from $\theta = 0^\circ$ to 90° . For slit-like hole arrays, the transmitted light was green at $\theta = 0^\circ$, green-orange at 45° , and red-orange at 90° (Figure 8e).

PLASMONIC PARTICLES

Metal and Dielectric Nanoparticles

Taking advantage of their free-standing nature, we used Au nanohole films as masks to fabricate macroscale areas of metal and dielectric particles (Figure 9a). If the mask is approximately

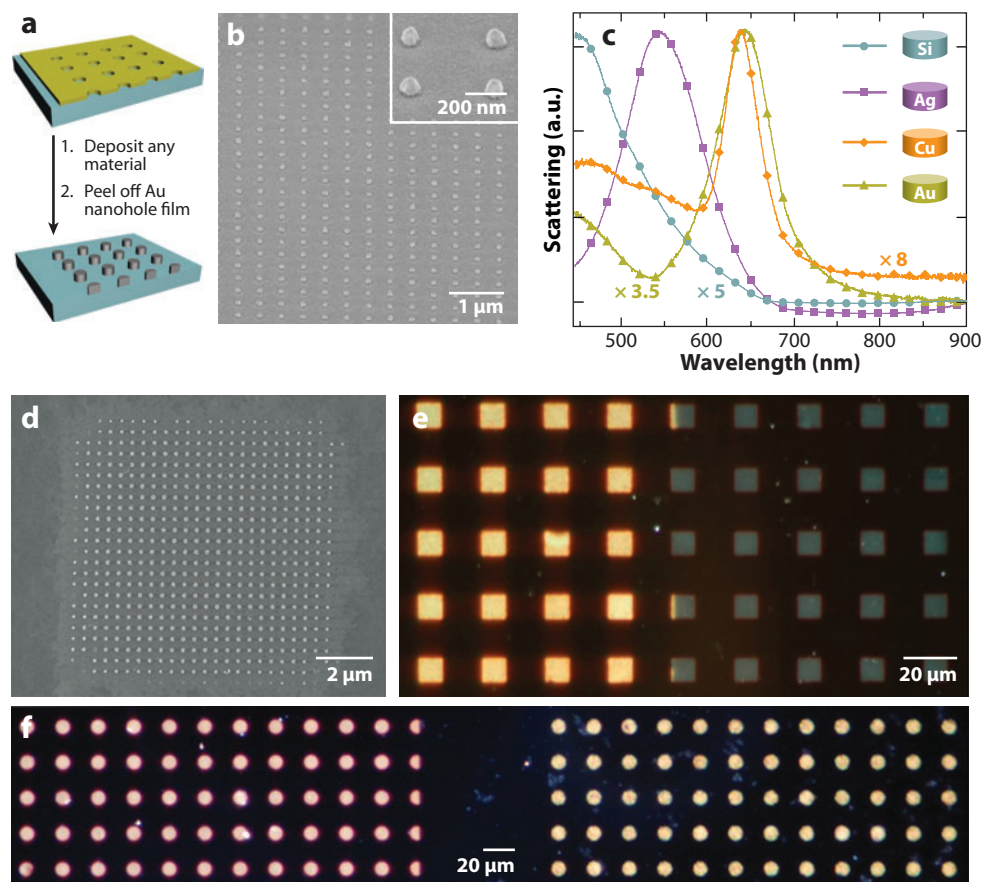


Figure 9

Infinite and multiscale nanoparticle arrays. (a) Scheme depicting the fabrication of nanoparticle arrays using soft-interference-lithography Au nanohole films as deposition masks. (b) Au nanoparticle array ($b = 50$ nm) fabricated using an infinite nanohole film; the inset shows a zoomed-in image. (c) Dark-field (DF) scattering spectra for metal (Ag, Cu, and Au) and dielectric (Si) nanoparticles ($b = 50$ nm). (d) 10×10 - μm square of Au nanoparticles ($b = 65$ nm) fabricated using a nanohole patch film with a 25 - μm pitch. (e) DF scattering image of Cu (left) and Ag (right) nanoparticles ($b = 15$ nm) fabricated on a different portion of the mask used in panel d. (f) DF scattering image of Au (left) and Ag (right) nanoparticles ($b = 65$ nm) fabricated using a 10 - μm circular nanohole patch film. Figure reproduced with permission from Reference 42, copyright (2007) Nature Publishing.

2 inches², over 10^{10} nanoparticles can be fabricated simultaneously. **Figure 9b** depicts a portion of an array of Au nanoparticles ($d = 100$ nm, $b = 50$ nm) supported on a glass substrate (no adhesion layer is necessary) with the same pitch ($a_0 = 400$ nm) as the SIL nanohole mask. We have used dark-field (DF) microscopy and spectroscopy to study the optical properties of the nanoparticles. White light incident from a DF condenser at high angles (approximately 53° – 71°) is scattered by the particles on a substrate, collected by an objective lens, and then projected onto a charge-coupled device imaging detector or analyzed using a grating spectrometer.

Nanoparticles of other single-component materials (Si, Ag, Cu) were fabricated and exhibited characteristic DF scattering peaks from UV to visible wavelengths (**Figure 9c**). In addition, Au films perforated with patches of nanoholes could be used as masks for multiscale patterning of different nanoparticles on the same substrate. **Figure 9d** shows an SEM image of an Au nanoparticle array generated from a single 10- μm square hole patch within a patch array ($a_0 = 25$ μm). A different portion of this patch array mask was also used to fabricate 100- μm^2 areas of thin ($b = 15$ nm) Cu and Ag nanoparticles side by side; DF scattering images indicated that some patches at the interface contained both materials (**Figure 9e**). Finally, **Figure 9f** shows that thicker ($b = 65$ nm) Au and Ag particles can be patterned into arrays of 10- μm circular regions.

Multilayered nanoparticles can also be fabricated by sequential deposition through SIL Au nanohole films (**Figure 10a**). We selected Au and alumina (Al_2O_3) as our building materials to investigate composite-metal nanoparticles. **Figure 10b** shows scattering spectra of three types of structures, all with Au layers 25 nm thick. The nanoparticles with two layers, Au/ Al_2O_3 ($b = 25/30$ nm) and $\text{Al}_2\text{O}_3/\text{Au}$ ($b = 55/25$ nm), exhibit single, dipolar resonance peaks of comparable widths, with the former occurring at longer wavelengths, as expected. The properties of nanoparticles in a sandwich structure (Au/ $\text{Al}_2\text{O}_3/\text{Au}$, $b = 25/30/25$ nm), with upper and lower layers identical to the two-layered nanoparticles above, support three peaks: two of the peaks are similar to those from the two-layered nanoparticles, whereas the third peak at shorter wavelengths ($\lambda = 600$ nm) might be attributed to coupling between the upper and lower Au disks or a hybridized plasmon resonance. Furthermore, we surrounded the nanoparticle arrays with different refractive-index oils to determine the evolution of their spectra. As expected, the dipolar LSP resonances shifted to longer wavelengths as n increased, and the apparent blue shift of the short wavelength peak from the sandwich structure (**Figure 10c**) could result from the appearance of a multipolar resonance.

Pyramidal Nanostructures

Serial lithographic techniques such as electron-beam lithography can fabricate structures with arbitrary sizes and shapes in two dimensions (31, 52), although low throughput and small write areas (hundreds of square micrometers) are current challenges. The deposition of materials through Au nanohole masks described above solves some scalability issues—and extends different materials combinations—but it does not solve the limitation of nanostructures with planar shapes. The PEEL process, however, enables an innovative approach for fabricating 3D nanostructures. At the same time that arrays of nanoholes are generated, pyramidal particles are formed directly beneath the holes and in the pyramidal pits of the Si substrate (**Figure 4**). This procedure thus provides a unique, template-based approach for generating monodisperse, anisotropic particles with smooth facets and sharp tips ($r < 2$ nm) with high densities (27).

Figure 11a displays arrays of Au pyramids supported by Si pedestals, which are achieved by anisotropic etching of the Si template (53) containing the pyramids. After releasing them on a flat substrate, the pyramids adopt two orientations: (*a*) with their tips pointing away from the surface (tip up) or (*b*) with their tips touching the surface (tip down). Previously, we found that Au pyramids

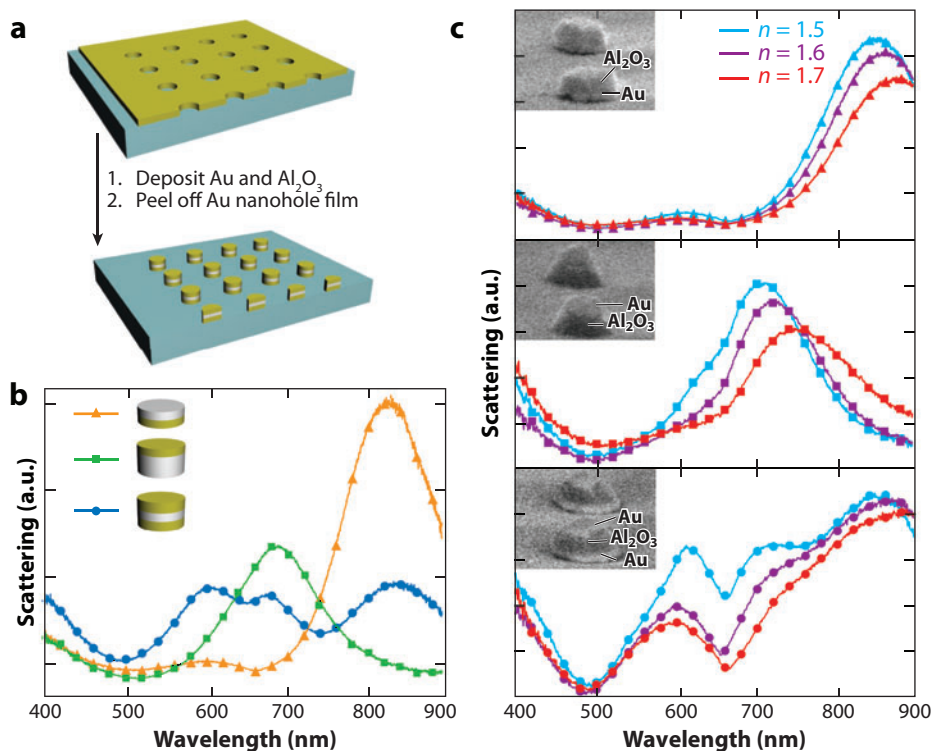


Figure 10

Multilayered metal and dielectric nanoparticles and refractive-index sensing. (a) Scheme depicting the fabrication of multilayered nanoparticle arrays using soft-interference-lithography Au nanohole films as deposition masks. (b) Dark-field (DF) scattering spectra for multilayered metal/dielectric nanoparticle arrays in air (refractive index, $n = 1$), Au/Al₂O₃ [$b = 25/30$ nm (orange triangles)], Al₂O₃/Au [$b = 55/25$ nm (green squares)], and Au/Al₂O₃/Au [$b = 25/30/25$ nm (blue circles)]. (c) DF scattering spectra of the multilayered nanoparticles in panel b surrounded by different refractive-index liquids. Figure reproduced with permission from Reference 42, copyright (2007) Nature Publishing.

with diameters $d = 100$ nm only supported a single dipolar resonance at approximately 720 nm (thickness $t = 50$ nm). The shape and location of the LSP resonance were in good agreement with discrete dipole approximation calculations (21). As their diameters increased from 200 nm to 300 nm ($t = 60$ nm), the pyramids started to develop structure in their scattering spectra (Figure 11b,c). First, as the diameter of the pyramid base became larger, the dipolar resonance shifted to longer wavelengths, and peaks and other structure emerged at approximately 600 nm. Second, the spectral features that blue-shifted relative to the dipolar resonance were more pronounced for 300-nm pyramids. Figure 11c indicates that the spectrum of tip-up pyramids is dominated by the resonance at approximately 600 nm, whereas tip-down pyramids exhibited a 600-nm peak with reduced intensity but an additional peak at NIR wavelengths. When the particles have sizes comparable with the wavelength of light, their optical resonances are sensitive to the direction of excitation, and certain excitation angles can make selected resonances more pronounced (23). For example, depending on the direction of incident light, the phase of the excitation field in asymmetric Au pyramids can vary significantly (21), which can result in the excitation of different superpositions of multipolar resonances (10).

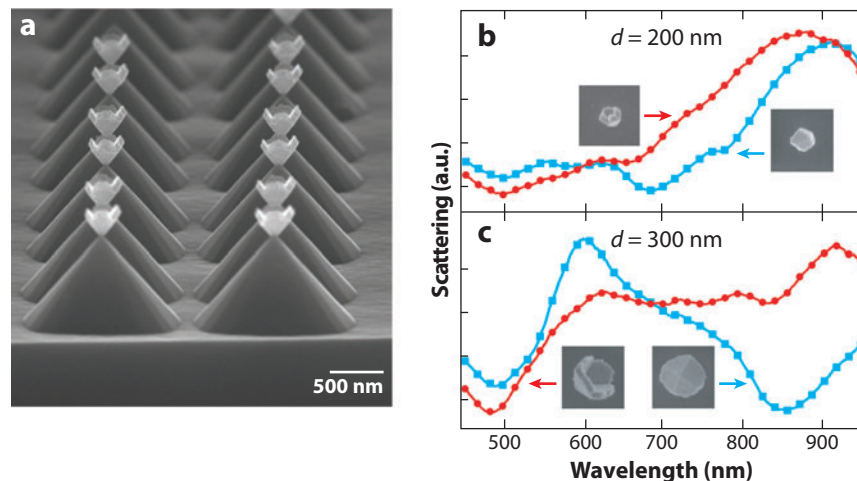


Figure 11

(a) Au pyramids supported on Si pedestals. Single-particle scattering spectra of 60-nm-thick Au pyramids with base diameters of (b) 200 nm and (c) 300 nm. Panels b and c reprinted with permission from Reference 55, copyright (2008) American Chemical Society.

The distinct scattering spectra of large ($d > 250$ nm) pyramids in different orientations (tip up and tip down) allow their orientation to be determined in condensed media without the need for direct and destructive imaging tools (54). For example, after randomly selecting and measuring the spectra of six bright spots in a DF image (Figure 12a), we found that their spectra fell into two categories: (a) those with 600-nm peaks of relatively high intensity and (b) those with peaks at

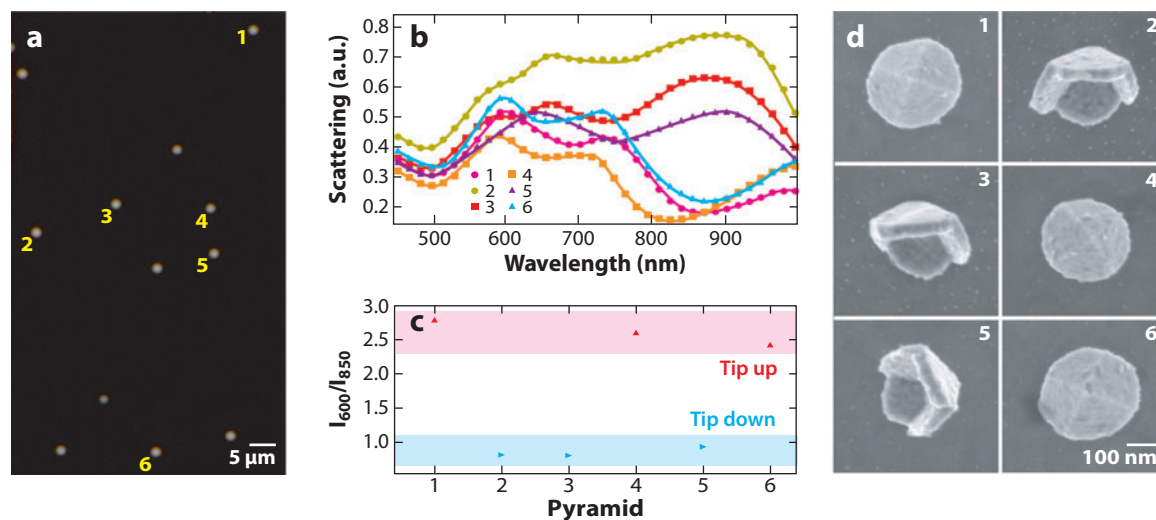


Figure 12

(a) Dark-field image of individual 300-nm Au pyramids on ITO/glass. (b) Single-particle scattering spectra of the pyramids indicated in panel a. (c) Ratio of intensities at 600 and 850 nm of the pyramids. (d) Scanning electron micrographs confirming the orientation of pyramids predicted by their spectra in panel b. Figure reprinted with permission from Reference 54, copyright (2007) American Chemical Society.

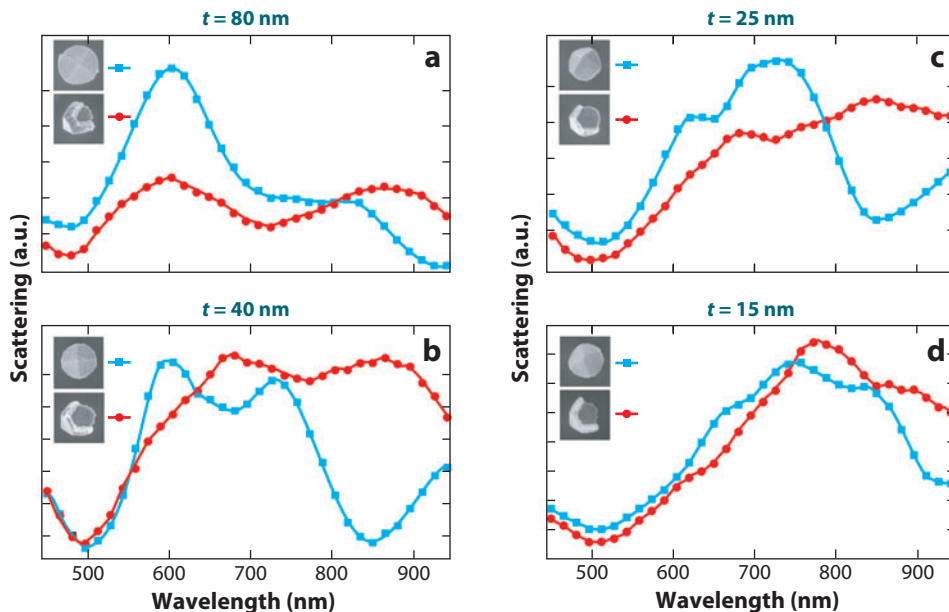


Figure 13

Scattering spectra of 300-nm Au pyramids with thicknesses of (a) 80 nm, (b) 40 nm, (c) 25 nm, and (d) 15 nm and with two orientations, tip up (blue squares) and tip down (red circles). Figure adapted and reprinted with permission from Reference 55, copyright (2008) American Chemical Society.

600 nm and 850 nm with comparable intensities (Figure 12b). Indeed, when the ratio of scattering intensities at 600 and 850 nm was calculated, two distinct bands emerged (Figure 12c). Scanning electron micrographs revealed that pyramids with high I_{600}/I_{850} ratios were tip up and those with low I_{600}/I_{850} ratios were tip down (Figure 12d).

To determine how the optical properties changed with the thickness of the pyramidal shells, we measured scattering spectra of pyramids with a fixed diameter ($d = 300$ nm) and with the thickness ranging from 15 nm to 80 nm (Figure 13). Notably, the tip-up and tip-down orientations of thicker pyramids exhibited more pronounced spectral differences than thinner pyramids of the two orientations (55). For tip-up pyramids, the intensity of the 600-nm peak increased as the thickness of the pyramids increased but seemed to disappear, or shift to longer wavelengths, when the thickness decreased. Moreover, as the thickness of the pyramidal shell approached $t = 15$ nm, all the resonances shifted to wavelengths greater than 650 nm (Figure 13d). Thus, besides their ability to support multipolar modes because of size, our pyramidal system can be tuned to exhibit multiple visible and NIR plasmon resonances simply by controlling the thickness of the metal deposition.

FUTURE OUTLOOK

Fundamental plasmonics research is laying the foundation for future technologies in diverse areas ranging from optics to electronics and imaging. To meet these challenges and advance the science, however, we need to simplify and scale the methods by which plasmonic nanostructures are constructed. Multiscale patterning—and SIL in particular—provides an important first step toward realizing new types of plasmonic architectures because (a) microscale ordering can be imposed

on the nanoscale patterns, and thus plasmonic coupling strengths can be tuned, and (b) the complexity of plasmonic metamaterials can be built up simply by starting with a different master. The prospect for multiscale plasmonic structures is considerably bright. In the short term, because they support intense and concentrated electromagnetic fields, plasmonic materials can be used for highly sensitive refractive-index sensing using films with arrays of nanoholes, as well as multiplexed, label-free detecting and screening of analytes using arrays of particles. In the long term, active or hybrid plasmonic materials will become important for understanding how plasmons can enhance or manipulate the properties of nonlinear media such as ferroelectric and optoelectronic materials. Furthermore, such materials combined with super-resolution imaging techniques could yield an unprecedented platform for studying biological processes within cells.

SUMMARY POINTS

1. Multiscale fabrication is important for designing new plasmonic systems to study the interplay of LSPs and SPPs, as well as SPPs with other SPPs.
2. SIL provides a scalable method for creating nanoscale patterns over macroscale dimensions.
3. PEEL is a new nanofabrication process that can simultaneously generate free-standing films perforated with nanoholes and 3D pyramidal particles.
4. Infinite subwavelength hole arrays exhibit sharp spectral features that change in relative amplitude and shift to longer wavelengths when exposed to increased refractive-index environments. These very narrow resonances can be attributed to SPPs on one side of the film coupling to a Wood's anomaly on the opposite side.
5. Gold nanohole arrays patterned into microscale patches exhibit strikingly different transmission properties. For example, patches of nanoholes display new, extremely narrow resonances that result in high refractive-index sensitivities.
6. Gold nanohole arrays can be used as deposition masks to create multicomponent arrays of nanoparticles on any surface without the need of an adhesion layer.
7. Nanofabricated pyramids are 3D asymmetric structures that exhibit orientation-dependent properties. This unique spectroscopic characteristic allows their orientation to be determined in condensed media.

DISCLOSURE STATEMENT

The authors are not aware of any biases that might be perceived as affecting the objectivity of this review.

ACKNOWLEDGMENTS

This work was supported by the National Science Foundation (NSF) under DMR-0705741, the MRSEC program at Northwestern University (DMR-0520513), the Center of Cancer Nanotechnology Excellence of the NIH National Cancer Institute under U54CA119341, and the David and Lucile Packard Foundation. This work used the *NUANCE* Center facilities, which are supported by NSF-MRSEC, NSF-NSEC, and the Keck Foundation. We thank our collaborators Jeffrey McMahon, Stephen K. Gray, and George C. Schatz for many useful discussions. T.W.O.

is the Dow Professor of Chemistry, a DuPont Young Professor, a Cottrell Scholar of Research Corporation, and an Alfred P. Sloan Research Fellow.

LITERATURE CITED

1. Odom TW, Nehl CL. 2008. How gold nanoparticles have stayed in the light: the 3M's principle. *ACS Nano* 2:612–16
2. **Ebbesen TW, Lezec HJ, Ghaemi HF, Thio T, Wolff PA. 1998. Extraordinary optical transmission through subwavelength hole arrays. *Nature* 391:667–69**
3. Lezec HJ, Degiron A, Devaux E, Linke RA, Martin-Moreno L, et al. 2002. Beaming light from a sub-wavelength aperture. *Science* 297:820–22
4. Grigorenko AN, Geim AK, Gleason HF, Zhang Y, Firsov AA, et al. 2005. Nanofabricated media with negative permeability at visible frequencies. *Nature* 438:335–38
5. **Dolling G, Wegener M, Soukoulis CM, Linden S. 2006. Negative-index metamaterial at 780 nm wavelength. *Opt. Lett.* 32:53–55**
6. Klein MW, Enkrich C, Wegener M, Linden S. 2006. Second-harmonic generation from magnetic metamaterials. *Science* 313:502–4
7. Kawata S. 2001. *Near-Field Optics and Surface Plasmon Polaritons*. Osaka, Japan: Springer
8. **Mock JJ, Barbic M, Smith DR, Schultz DA, Schultz S. 2002. Shape effects in plasmon resonance of individual colloidal silver nanoparticles. *J. Chem. Phys.* 116:6755–59**
9. Oldenburg SJ, Averitt RD, Westcott SL, Halas NJ. 1998. Nanoengineering of optical resonances. *Chem. Phys. Lett.* 288:243–47
10. **Shuford KL, Lee J, Odom TW, Schatz GC. 2008. Optical properties of gold pyramidal shells. *J. Phys. Chem. C* 112:6662–66**
11. Raether H. 1988. *Surface Plasmons*. Berlin: Springer
12. **Gao H, Henzie J, Odom TW. 2006. Direct evidence for surface plasmon-mediated enhanced light transmission through metallic nanohole arrays. *Nano Lett.* 6:2104–8**
13. Lamprecht B, Krenn JR, Schider G, Ditlbacher H, Salerno M, et al. 2001. Surface plasmon propagation in microscale metal stripes. *Appl. Phys. Lett.* 79:51
14. Daniel M-C, Astruc D. 2004. Gold nanoparticles: assembly, supramolecular chemistry, quantum-size-related properties, and applications toward biology, catalysis, and nanotechnology. *Chem. Rev.* 104:293–346
15. Xia Y, Halas NJ. 2005. Shape-controlled synthesis and surface plasmonic properties of metallic nanostructures. *MRS Bull.* 30:338–48
16. Haes AJ, Haynes CL, McFarland AD, Schatz GC, Van Duyne RP, Zou S. 2005. Plasmonic materials for surface-enhanced sensing and spectroscopy. *MRS Bull.* 30:368–75
17. Bohren CF, Huffman DR. 1998. *Absorption and Scattering of Light by Small Particles*. New York: Wiley
18. Kumbhar AS, Kinnan MK, Chumanov G. 2005. Multipole plasmon resonances of submicron silver particles. *J. Am. Chem. Soc.* 127:12444–45
19. Millstone JE, Park S, Shuford KL, Qin L, Schatz GC, Mirkin CA. 2005. Observation of a quadrupole plasmon mode for a colloidal solution of gold nanoprisms. *J. Am. Chem. Soc.* 127:5312–13
20. Shuford KL, Ratner MA, Schatz GC. 2005. Multipolar excitation in triangular nanoprisms. *J. Chem. Phys.* 123:114713
21. **Henzie J, Shuford KL, Kwak E-S, Schatz GC, Odom TW. 2006. Manipulating the optical properties of pyramidal nanoparticle arrays. *J. Phys. Chem. B* 110:14028**
22. Kelly KL, Coronado E, Zhao LL, Schatz GC. 2003. The optical properties of metal nanoparticles: the influence of size, shape, and dielectric environment. *J. Phys. Chem. B* 107:668–77
23. Krenn JR, Schider G, Rechberger W, Lamprecht B, Leitner A, et al. 2000. Design of multipolar plasmon excitations in silver nanoparticles. *Appl. Phys. Lett.* 77:3379–81
24. Jain PK, Lee KS, El-Sayed IH, El-Sayed MA. 2006. Calculated absorption and scattering properties of gold nanoparticles of different size, shape, and composition: applications in biological imaging and biomedicine. *J. Phys. Chem. B* 110:7238–48
2. First report of enhanced optical transmission through subwavelength hole arrays.
5. First report of a plasmonic metamaterial with a negative refractive index at visible wavelengths.
8. First experiment that combined spectroscopy with high-resolution transmission electron microscopy to confirm the importance of particle shape on surface plasmon resonances.
10. Theoretical calculations that identified the multipolar plasmon resonances of Au pyramids at visible and NIR wavelengths.
12. Confirmed that surface plasmons were responsible for enhanced optical transmission through subwavelength hole arrays.
21. Showed that plasmon resonances of anisotropic particles were sensitive to both polarization and wave vector.

42. Introduced SIL as a high-throughput, materials-general nanofabrication method of plasmonic substrates, such as arrays of nanoholes and nanoparticles.

44. Revealed that microscale arrays of nanoholes support high-order SPP Bloch waves and that anisotropic nanoholes exhibit polarization-dependent color.

45. First paper to describe the fabrication of free-standing nanohole arrays using PEEL.

25. Murphy CJ, Sau TK, Gole AM, Orendorff CJ, Gao J, et al. 2005. Anisotropic metal nanoparticles: synthesis, assembly, and optical applications. *J. Phys. Chem. B* 109:13857–70
26. Wiley B, Sun Y, Chen J, Cang H, Li Z, et al. 2005. Shape-controlled synthesis of silver and gold nanostructures. *MRS Bull.* 30:356–61
27. Henzie J, Kwak E-S, Odom TW. 2005. Mesoscale metallic pyramids with nanoscale tips. *Nano Lett.* 5:1199–202
28. Schimid H, Michel B. 2000. Siloxane polymers for high-resolution, high-accuracy soft lithography. *Macromolecules* 33:3042–49
29. Xia Y, Whitesides GM. 1998. Soft lithography. *Annu. Rev. Mater. Sci.* 28:153–84
30. Xu Q, Tonks I, Fuerstman MJ, Love JC, Whitesides GM. 2004. Fabrication of free-standing metallic pyramidal shells. *Nano Lett.* 4:2509–11
31. Hicks EM, Zou S, Schatz GC, Spears KG, Van Duyne RP, et al. 2005. Controlling plasmon line shapes through diffractive coupling in linear arrays of cylindrical nanoparticles fabricated by electron beam lithography. *Nano Lett.* 5:1065–70
32. Haynes CL, McFarland AD, Zhao L, Van Duyne RP, Schatz GC, et al. 2003. Nanoparticle optics: the importance of radiative dipole coupling in two-dimensional nanoparticle arrays. *J. Phys. Chem. B* 107:7337–42
33. Gunnarsson L, Rindzevicius T, Prikulis J, Kasemo B, Kall M, et al. 2005. Confined plasmons in nanofabricated single silver particle pairs: experimental observations of strong interparticle interactions. *J. Phys. Chem. B* 109:1079–87
34. Grupp DE, Lezec HJ, Thio T, Ebbesen TW. 1999. Beyond the Bethe limit: tunable enhanced light transmission through a single sub-wavelength aperture. *Adv. Mater.* 11:860–62
35. Shumaker-Parry JS, Rochholz H, Kreiter M. 2005. Fabrication of crescent-shaped optical antennas. *Adv. Mater.* 17:2131–34
36. Liu GL, Lu Y, Kim J, Doll JC, Lee LP. 2005. Magnetic nanocrescents as controllable surface-enhanced Raman scattering nanoprobe for biomolecular imaging. *Adv. Mater.* 17:2683–88
37. Haes AJ, Zhao J, Zou S, Own CS, Marks LD, et al. 2005. Solution-phase, triangular Ag nanotriangles fabricated by nanosphere lithography. *J. Phys. Chem. B* 109:11158–62
38. Nicewarner-Pena SR, Freeman RG, Reiss BD, He L, Pena DJ, et al. 2001. Submicrometer metallic barcodes. *Science* 294:137–41
39. Odom TW, Love JC, Paul KE, Wolfe DB, Whitesides GM. 2002. Improved pattern transfer in soft lithography using composite stamps. *Langmuir* 18:5314–20
40. Odom TW, Thalladi VR, Love JC, Whitesides GM. 2002. Generation of 30–50 nm structure using easily fabricated, composite PDMS masks. *J. Am. Chem. Soc.* 124:12112–13
41. Gates BD, Xu Q, Love CJ, Wolfe DB, Whitesides GM. 2004. Unconventional nanofabrication. *Annu. Rev. Mater. Res.* 34:339–72
42. Henzie J, Lee MH, Odom TW. 2007. Multiscale patterning of plasmonic metamaterials. *Nat. Nanotechnol.* 2:549–54
43. Greyson EC, Babayan Y, Odom TW. 2004. Directed growth of ordered arrays of small-diameter ZnO nanowires. *Adv. Mater.* 16:1348–52
44. Lee MH, Gao H, Henzie J, Odom TW. 2007. Microscale arrays of nanoscale holes. *Small* 3:2029–33
45. Kwak ES, Henzie J, Chang SH, Gray SK, Schatz GC, Odom TW. 2005. Surface plasmon standing waves in large-area subwavelength hole arrays. *Nano Lett.* 5:1963–67
46. Bethe HA. 1944. Theory of diffraction by small holes. *Phys. Rev.* 66:163–82
47. Genet C, Ebbesen TW. 2007. Light in tiny holes. *Nature* 445:39–46
48. Barnes WL, Murray WA, Dintinger J, Devaux E, Ebbesen TW. 2004. Surface plasmon polaritons and their role in the enhanced transmission of light through periodic arrays of subwavelength holes in a metal film. *Phys. Rev. Lett.* 92:107401
49. Chang S-H, Gray SK, Schatz GC. 2005. Surface plasmon generation and light transmission by isolated nanoholes and arrays of nanoholes in thin metal films. *Opt. Expr.* 13:3150–65
50. Wood RW. 1935. Anomalous diffraction gratings. *Phys. Rev.* 48:928–36

51. McMahon JM, Henzie J, Odom TW, Gray SK, Schatz GC. 2007. Tailoring the sensing capabilities of nanohole arrays in gold films with Wood's anomaly-surface plasmon polaritons. *Opt. Expr.* 15:18119-29
52. Canfield BK, Kujala S, Kauranen M, Jefimovs K, Vallius T, Turunen J. 2005. Remarkable polarization sensitivity of gold nanoparticle arrays. *Appl. Phys. Lett.* 86:183109
53. Seidel H, Csepregi L, Heuberger A, Baumgärtel H. 1990. Anisotropic etching of crystalline silicon in alkaline solutions. *J. Electrochem. Soc.* 137:3612-26
54. Hasan W, Lee J, Henzie J, Odom TW. 2007. Selective functionalization and spectral identification of Au nanopyramids. *J. Phys. Chem. C* 111:17176-79
55. Lee J, Hasan W, Stender CL, Odom TW. 2008. **Pyramids: a platform for designing multifunctional plasmonic particles.** *Acc. Chem. Res.* In press; doi: 10.1021/ar800126p
56. Wiley B, Sun Y, Mayers B, Xia Y. 2004. Shape-controlled synthesis of metal nanostructures: the case of silver. *Chemistry* 11:454-63
57. Jana NR, Gearheart L, Murphy CJ. 2001. Wet chemical synthesis of silver nanorods and nanowires of controllable aspect ratio. *Chem. Commun.* 7:617-18

55. Review on the fabrication, surface functionalization, and optical properties of pyramidal metal particles.



Contents

Frontispiece	xiv
Sixty Years of Nuclear Moments <i>John S. Waugh</i>	1
Dynamics of Liquids, Molecules, and Proteins Measured with Ultrafast 2D IR Vibrational Echo Chemical Exchange Spectroscopy <i>M.D. Fayer</i>	21
Photofragment Spectroscopy and Predissociation Dynamics of Weakly Bound Molecules <i>Hanna Reisler</i>	39
Second Harmonic Generation, Sum Frequency Generation, and $\chi^{(3)}$: Dissecting Environmental Interfaces with a Nonlinear Optical Swiss Army Knife <i>Franz M. Geiger</i>	61
Dewetting and Hydrophobic Interaction in Physical and Biological Systems <i>Bruce J. Berne, John D. Weeks, and Rubong Zhou</i>	85
Photoelectron Spectroscopy of Multiply Charged Anions <i>Xue-Bin Wang and Lai-Sheng Wang</i>	105
Intrinsic Particle Properties from Vibrational Spectra of Aerosols <i>Ómar F. Sigurbjörnsson, George Firasescu, and Ruth Signorell</i>	127
Nanofabrication of Plasmonic Structures <i>Joel Henzie, Jeunghoon Lee, Min Hyung Lee, Warefta Hasan, and Teri W. Odom</i>	147
Chemical Synthesis of Novel Plasmonic Nanoparticles <i>Xianmao Lu, Matthew Rycenga, Sara E. Skrabalak, Benjamin Wiley, and Younan Xia</i>	167
Atomic-Scale Templates Patterned by Ultrahigh Vacuum Scanning Tunneling Microscopy on Silicon <i>Michael A. Walsb and Mark C. Hersam</i>	193
DNA Excited-State Dynamics: From Single Bases to the Double Helix <i>Chris T. Middleton, Kimberly de La Harpe, Charlene Su, Yu Kay Law, Carlos E. Crespo-Hernández, and Bern Kobler</i>	217

Dynamics of Light Harvesting in Photosynthesis <i>Yuan-Chung Cheng and Graham R. Fleming</i>	241
High-Resolution Infrared Spectroscopy of the Formic Acid Dimer <i>Özgür Birer and Martina Havenith</i>	263
Quantum Coherent Control for Nonlinear Spectroscopy and Microscopy <i>Yaron Silberberg</i>	277
Coherent Control of Quantum Dynamics with Sequences of Unitary Phase-Kick Pulses <i>Luis G.C. Rego, Lea F. Santos, and Victor S. Batista</i>	293
Equation-Free Multiscale Computation: Algorithms and Applications <i>Ioannis G. Kevrekidis and Giovanni Samaey</i>	321
Chirality in Nonlinear Optics <i>Levi M. Hupert and Garth J. Simpson</i>	345
Physical Chemistry of DNA Viruses <i>Charles M. Knobler and William M. Gelbart</i>	367
Ultrafast Dynamics in Reverse Micelles <i>Nancy E. Levinger and Laura A. Swafford</i>	385
Light Switching of Molecules on Surfaces <i>Wesley R. Browne and Ben L. Feringa</i>	407
Principles and Progress in Ultrafast Multidimensional Nuclear Magnetic Resonance <i>Mor Mishkovsky and Lucio Frydman</i>	429
Controlling Chemistry by Geometry in Nanoscale Systems <i>L. Lizana, Z. Konkoli, B. Bauer, A. Jesorka, and O. Orwar</i>	449
Active Biological Materials <i>Daniel A. Fletcher and Phillip L. Geissler</i>	469
Wave-Packet and Coherent Control Dynamics <i>Kenji Ohmori</i>	487

Indexes

Cumulative Index of Contributing Authors, Volumes 56–60	513
Cumulative Index of Chapter Titles, Volumes 56–60	516

Errata

An online log of corrections to *Annual Review of Physical Chemistry* articles may be found at <http://physchem.annualreviews.org/errata.shtml>